NOISE RADAR PERFORMANCE

UDC 621.37

TIME AND RANGE ACCURACY OF SHORT-RANGE ULTRA-WIDEBAND PSEUDO-NOISE RADAR, NRT-2012

J. SACHS, R. HERRMANN, AND M. KMEC

Time and range estimations based on ultra-wideband (UWB) measurements need to be carefully considered with respect to their accuracy, since range, propagation delay and time position can often not be uniquely defined. The paper illustrates these issues and shows some common approaches for UWB range and time position estimation. Ranging errors provoked from the sensor device are introduced and the performance of pseudo-noise radar concepts is shown. They provide excellent time axis accuracy due to a stable clock reference and cause random timing errors in the fs-range which is a consequence of a robust synchronization concept and jitter suppression by correlation. The impact of frequency aliasing onto time position measurements is considered as well.

Keywords: PN-sequence, jitter, time position, range accuracy, correlation, aliasing.

1. INTRODUCTION

The target range or time of flight are the most important parameters gained from a radar measurement. The goal of this paper is to discuss the achievable precision and some error sources of such measurements using ultra-wideband (UWB) radar devices. Specifically, we will focus on UWB pseudo noise (PN) radar for short range applications.

Precise and stable time or range measurements are important for applications involving super-resolution techniques [1], micro motion detection [2], target localization [3], system calibration [4, 5], hidden target detection [6] and others. The attached references refer to corresponding examples.

In what follows, we start with an introduction of range measurements and the general challenges one is faced in case of UWB sounding. Furthermore, we consider some methods and errors of pulse position estimation. In our discussion, we mainly refer to a PN-radar principle and investigate its robustness against deterministic and random errors.

2. STATEMENT OF THE PROBLEM

2.1. Experimental setup

Here we are mainly interested in two points. Firstly, it refers to the question how precise we can determine the range of a target.

This point is identical with the question how precise we can measure a time delay $\Delta\tau$ (propagation speed of the sounding waves is supposed to be exactly known). We will focus our consideration to a single target scenario, i.e. the issues of range resolution and the separation of two closely located targets will be not within the scope of the paper. The second point relates to the detection of weak targets closely located behind a penetrable but strongly reflecting interface. We refer to the issues related to range measurements by the term scenario A and for hidden target detection we take scenario B.

Range estimation based on radar sensing is illustrated in Fig. 1. A sounding wave is emitted by an antenna, reflected by the target and collected by the same (compare Fig. 1a) or a second antenna. The roundtrip time is determined from the mutual delay $\Delta\tau$ between received and transmitted signals. The relation

$$\hat{R} = \frac{1}{2}\Delta\tau\, c_0 \quad \text{with} \quad \Delta\tau = \tau_y - \tau_x - 2\tau_0 \tag{1}$$

(c_0 – speed of light; τ_0 – antenna internal propagation delay) is then usually taken as an estimation for the target's distance R_0, i.e. one assumes $R_0 \triangleq \hat{R}$.

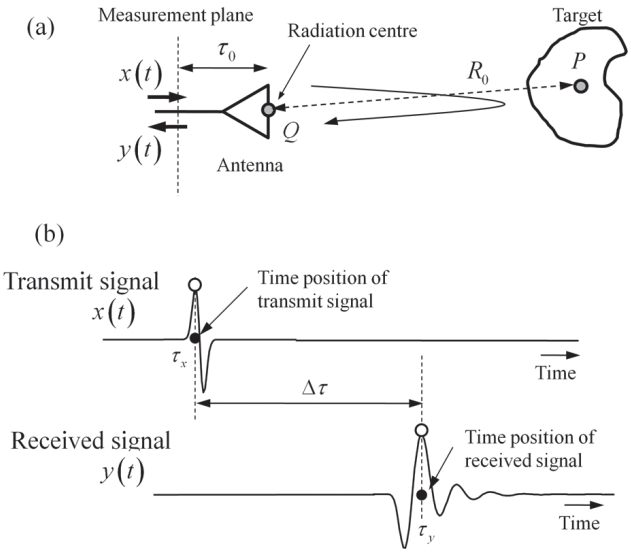

Fig. 1. Principle of range estimation based on radar measurements for scenario A: (a) measurement setup; (b) simplified UWB signals

Hidden target detection (scenario B) is symbolized in Fig. 2. If the target is located close to a boundary, the surface reflex (also denoted as surface clutter) will overwhelm the target return and the question is, to what extend we can remove the strong reflex from the captured signal and detect the target. In two cases

this would be at least theoretically perfectly possible – namely if we can take a reference measurement from the interface without target or if the target shows some temporal variations (movement, shape variation, permittivity) while the interface stays time invariant.

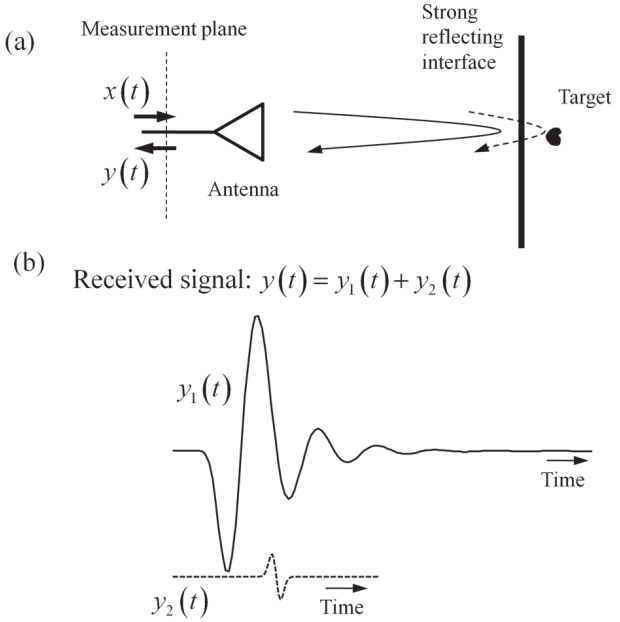

Fig. 2. Hidden target detection in scenario B: (a) measurement setup; (b) returned UWB signals

By considering these scenarios more profoundly under the aspect of ultra-wideband sensing, we will become aware of some shortcomings and insufficiencies which are discussed below.

2.2. Range definition

In case of scenario A, it already starts with the definition of the target range. Mathematically correct, the range assigns the distance between two points, i.e. two infinitesimal small "objects". By introducing a side condition as "shortest range", we can still define uniquely the distance between a point and a straight line (e.g. a thin wire or a "knife" edge) or a point and a flat plane. Hence, the prerequisite for a unique range measurement is only given if the involved objects (i.e. antenna and target) are at least in one dimension infinitesimal small. But practically, this will be commonly not the case.

Since the achievable range resolution of UWB sensors is often better than the geometric size of the involved objects, these issues have to be appropriately respected. In case of the antenna, this can be done by introducing a centre of radiation (refer to point Q in Fig. 1) by prior calibration [7, 8]. It "merges" the properties of a real object with finite dimensions in a virtual point. The determination of a more or less objective "scattering centre" for the target (exemplified by point P in Fig. 1) is barely possible since the scattering object is usually not known a-priori.

2.3. Definition of Roundtrip time

The determination of the roundtrip or delay time $\Delta\tau$ is linked to a similar problem. $\Delta\tau$ is a time interval which is defined by the elapsed time between two time points. Thus, we need again "points", but what we have are signals of finite duration (or finite coherence time) due to limited bandwidth. Hence, we either have to define the time positions τ_x, τ_y of two pulses (transmitted and received one) or we have to estimate the time position of the cross-correlation maximum from $x(t)$ and $y(t)$.

Both approaches face the same problem since an exact time delay may only be defined between two signals of identical shape (i.e. the fidelity [8, 9] of both signals must be one). While $x(t)$ may be obtained from a calibration or reference measurement, $y(t)$ usually remains unpredictable due to the unknown scatterer (except when the scatterer approximates a small point, an infinite line, or infinite plane where exact mathematical models are known). Hence, we have to anticipate increasing systematic errors if the fidelity departs from one.

Further challenges arise if the return signal of the target is affected by noise, multipath signals, or other clutter. The interested reader can find some discussions on these topics in [10, 11]. Since our main aim is to investigate the role of the measurement device in range measurements, we will not go deeper into issues from above since they are mainly motivated by the conditions of the test scenario. That is, we assume in our following consideration that we have measurement conditions which allow defining uniquely the radar rage. An example scenario could e.g. be the scattering from an infinite metal sheet.

2.4. Pulse Position

Independently on how delay time measurements are performed or on how strong they are affected by different signals and perturbations, they are always connected with the determination of at least one pulse position.

There are multifold options to define the pulse position. The most popular strategies are

1) to use the intersection of the rising or falling pulse edge with an absolute or normalized threshold (e.g. normalized to the pulse peak)

2) to take the maximum position of the pulse. This approach is a special case of 1) since the maximum position is achieved if the first derivative of the pulse form crosses the zero line. Note that this method may be extended to complex valued impulse waveforms as they appear after IQ-down-conversion of band-pass signals (complex envelope).

3) to take the zero crossing of the strongest half-cycle in the case of a band-pass pulse. The selection of the correct half-cycle may be based on the maximum position of the pulse envelope.

4) to determine one of the centers of gravity:

$$\tau_p = \frac{\int t\left|x(t)\right|^p dt}{\int \left|x(t)\right|^p dt}; \quad p \geq 1 \tag{2}$$

It follows from eq. (2) that τ_1 relates to the gravity centre of the pulse area, τ_2 represents the energetic centre of the pulse, and τ_∞ offers a second possibility to define the maximum position.

The pros and cons of the different definitions of pulse position are compared in [8]. In summary of the discussion there, we can state that threshold crossing of either the first derivative (i.e. maximum position) or of the original pulses or cross-correlation function provides the best performance in case of baseband signals (pulse or pseudo noise). The integral values of pulse position corresponding to point 4 are prone to biased estimations if the signal is affected by noise.

Using the "maximum approach" (point 2), we find for the variance φ_0^2 of time delay estimation [8]:

$$\varphi_0^2 = \frac{\underset{\cdot\cdot}{B}_n^2}{3(4\pi)^2 \, SNR \, \underset{\cdot\cdot}{B}_{eff}^4}, \qquad (3)$$

$\underset{\cdot\cdot}{B}_n$ — noise bandwidth of the receiver (double sided); SNR — SNR value of the receiving signal; $B_{eff}^2 = \int f^2 \underset{\cdot\cdot}{\Psi}_{yy}(f) df \Big/ \int \underset{\cdot\cdot}{\Psi}_{yy}(f) df$ — effective bandwidth of the receiving signal; $\underset{\cdot\cdot}{\Psi}_{yy}(f)$ — power spectrum of receiving signal (double sided).

For optimum noise suppression, the receiver bandwidth should be matched to the bandwidth of the input signal. If this is of constant power spectral density within the spectral band $\pm \underset{\cdot\cdot}{B}/2$ which equals the receiver noise bandwidth, eq. (3) modifies to:

$$\varphi_0^2 = \frac{1}{\left(2\pi B_{eff}\right)^2 SNR} = \frac{3}{\pi^2 \underset{\cdot\cdot}{B}^2 SNR} \qquad (4)$$

$$for \quad \underset{\cdot\cdot}{\Psi}_{yy}(f) = \begin{cases} \Psi_0 & |f| \le \underset{\cdot\cdot}{B}_n/2 \\ 0 & |f| > \underset{\cdot\cdot}{B}_n/2 \end{cases} \Rightarrow B_{eff}^2 = \frac{\underset{\cdot\cdot}{B}_n^2}{12}$$

In what follows, we will investigate the role of the sensing device for the correct determination of the pulse position corresponding to scenario A as well as the conditions allowing precise suppression of the interface reflex from scenario B.

3. PRECISE AND STABLE DEVICE TIMING

It is obvious from the discussions of section 2.4, that imperfections of the device internal time representation as well as additive random noise will be the major sources of time position errors. Since nowadays the captured signals are usually digitized, we have to anticipate following timing errors:

- an erroneous value of the sampling interval (e.g. caused from an unreliable clock generator)
- systematic deviations from an equidistant sampling interval. Such deviations may have a global tendency leading to a non-linear time axis of the device or they are arbitrary so that they generate a kind of "systematic" jitter. The first effect may be observed in e.g. sequential sampling oscilloscopes which use a dual ramp approach for sampling control. The second effect appears if the dual ramp approach is replaced by digitally controlled stepped delay lines whose delay steps are not ideally identical [8].
- random deviations of the sampling points (sampling jitter)
- random fluctuations of stimulus launch (trigger jitter).

Fig. 3 (a) represents a sensor concept which defeats these timing errors. It is based on the generation of UWB PN-signals to stimulate the device under test (DUT) and a sub-sampling receiver [12].

The timing of the whole device is controlled by a single tone RF-clock operating commonly in the 2-20 GHz range. Such a generator can be built for very precise frequency values and low phase noise. This provides one of the prerequisites for absolute timing accuracy and low random timing errors.

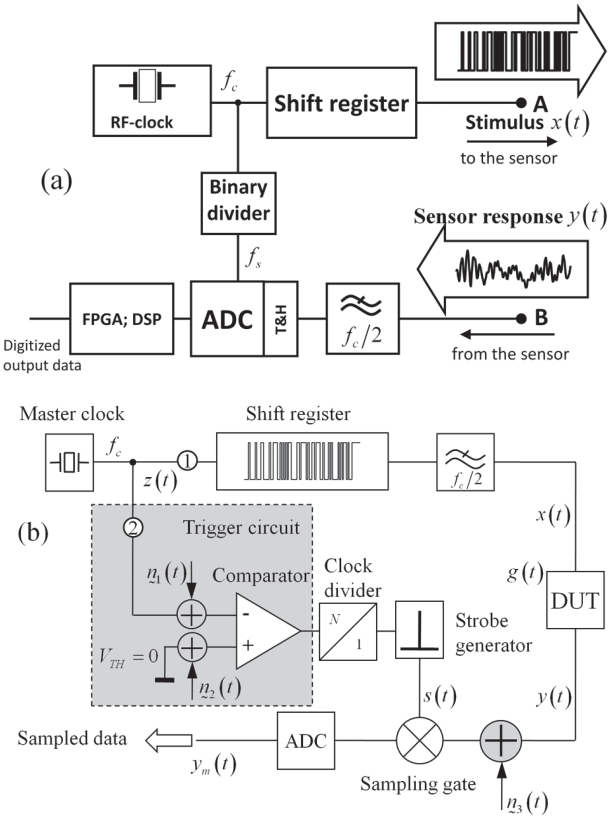

Fig. 3. Block schematic (a) of a PN-sequence ultra-wideband sensor and its simplified system model (b)

A major issue is to trigger the signal generator (i.e. the shift register) and the Track and hold circuit (T&H) as reliable as possible. We will discuss this point with help of Fig. 3 (b). For the sake of shortness, we only refer to a single jitter source, namely the aperture jitter of the strobe signal $s(t)$. We model it by the grey box of Fig. 3 (b). Two noise voltages $\underset{\sim}{n}_1(t) \sim N\left(0, \sigma_1^2\right)$ and $\underset{\sim}{n}_2(t) \sim N\left(0, \sigma_2^2\right)$ are transformed into jitter by the comparator. The binary divider is then assumed to be jitter free.

The noise signals $\underset{\sim}{n}_1(t)$ and $\underset{\sim}{n}_2(t)$ provoke a random temporal fluctuation $\Delta\underset{\sim}{\tau}_j$ of comparator switching which we regard as a zero mean random process having the probability density function (PDF) $p_{\Delta\tau}(t)$. The period should be placed into the previous line. Hence, we have for the expected value:

$$\mathrm{E}\left\{\Delta\tilde{\tau}_j\right\} = \int_{-\infty}^{\infty} t\, p_{\Delta\tau}(t)\,\mathrm{d}t = 0 \tag{5}$$

The variance of the fluctuations follows from simple considerations to be:

$$\begin{aligned}\mathrm{var}\left\{\Delta\tilde{\tau}_j\right\} = \varphi_T^2 &= \int_{-\infty}^{\infty} t^2\, p_{\Delta\tau}(t)\,\mathrm{d}t \\ &\approx \frac{\sigma_1^2+\sigma_2^2}{\left(\left.\dfrac{\mathrm{d}\,z(\xi)}{\mathrm{d}\,\xi}\right|_{\xi=t_0}\right)^2}\end{aligned} \tag{6}$$

whereat t_0 represents the nominal trigger point at which the unperturbed trigger signal $z(t)$ crosses the threshold V_{TH}.

In our case, we have a sine wave generator as trigger source and the threshold level is zero $V_{TH} = 0$. Hence we get from (6):

$$\varphi_T^2 = \frac{\sigma_1^2+\sigma_2^2}{(2\pi f_c)^2} \tag{7}$$

Now, we can model the captured signal as a random process (for the sake of convenience, we will stay at time continuous signals and consider the DUT as a simple delay, i.e. $g(t) = \delta(t-\Delta\tau)$):

$$\begin{aligned}\tilde{y}_m(t) &= \tilde{y}\left(t+\Delta\tilde{\tau}_j\right) + \tilde{n}_3\left(t+\Delta\tilde{\tau}_j\right) \\ &= \sum_{\nu}\frac{1}{\nu!}\left(\frac{\mathrm{d}^\nu y(\xi)}{\mathrm{d}\,\xi^\nu}+\frac{\mathrm{d}^\nu n_3(\xi)}{\mathrm{d}\,\xi^\nu}\right)\Bigg|_{\xi=t}\Delta\tilde{\tau}_j^\nu \\ &\approx y(t)+\left.\frac{\mathrm{d}\,y(\xi)}{\mathrm{d}\,\xi}\right|_{\xi=t}\Delta\tilde{\tau}_j+\tilde{n}_3(t) \\ &\approx x(t-\Delta\tau)+\left.\frac{\mathrm{d}\,x(\xi)}{\mathrm{d}\,\xi}\right|_{\xi=t-\Delta\tau}\Delta\tilde{\tau}_j+\tilde{n}_3(t)\end{aligned} \tag{8}$$

The order of Taylor series expansion in eq. (8) can be drastically reduced if jitter and noise do not dominate the deterministic part of the signal.

We will use this relation, to estimate the jitter φ_T^2 of an M-sequence device [13]. For that purpose, we need to know the signal derivative at any time point. Since M-sequence devices are Nyquist sampled, the equivalent sampling rate has to be increased in order to permit reliable derivation. Therefore, we introduced a mechanical precision delay line at points ①, ② (see Fig. 3 (b)) or as a DUT. The delay steps are 0.2 ps allowing an equivalent sampling rate of 5 THz. Thus, the realizations of $\tilde{y}_m(t)$ can be considered as quasi continuous in time. Furthermore, the random perturbations have to be suppressed before the derivation can be determined. This was done by synchronous averaging of about $N = 100$ realizations of $\tilde{y}_m(t)$:

$$\begin{aligned}\bar{y}_m(t) &= \frac{1}{N}\sum_{n=1}^{N}\tilde{y}_{m,n}(t) \\ &= \frac{1}{N}\sum_{n=1}^{N}\left(x_n\left(t-\Delta\tau+\Delta\tilde{\tau}_{j,n}\right)+\tilde{n}_{3,n}\left(t+\Delta\tilde{\tau}_{j,n}\right)\right)\end{aligned} \tag{9}$$

Its expected value leads to the relation:

$$\begin{aligned}\mathrm{E}\left\{\bar{y}_m(t)\right\} &= x(t-\Delta\tau) * p_{\Delta\tau}(t) \\ &\approx x(t-\Delta\tau) \quad \textit{if} \quad \varphi_T\, B \ll 1\end{aligned} \tag{10}$$

such that $\bar{y}_m(t)$ can be considered as a reasonable source to calculate the signal derivative in particular if the convolution may be omitted. This is allowed if the temporal width φ_T of $p_{\Delta\tau}(t)$ is short compared to any variations in $x(t)$ which we have expressed by the side condition $\varphi_T\, B \ll 1$.

Using eq. (8), the variance of the captured signal can be written as:

$$\begin{aligned}\mathrm{var}\left\{\tilde{y}_m(t)\right\} &= \sigma_y^2(t) = \sigma_\varphi^2(t)+\sigma_3^2 \\ &= \left(\left.\frac{\mathrm{d}\,x(\xi)}{\mathrm{d}\,\xi}\right|_{\xi=t-\Delta\tau}\right)^2\varphi_T^2+\sigma_3^2\end{aligned} \tag{11}$$

with $\tilde{n}_3 \sim N\left(0,\sigma_3^2\right)$

If we plot for all samples of the signal the standard deviation $\sigma_y(t_0)$ versus the slope of the signal $\mathrm{d}\bar{y}_m(t)/\mathrm{d}t\big|_{t=t_0}$ ($t_0 \in [0,T)$; T — signal period), we can expect behaviour as depicted in Fig. 4.

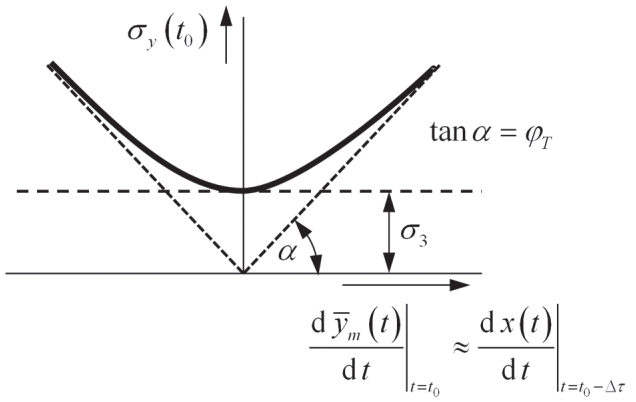

Fig. 4. Illustration of signal variance as function of signal slope under the presence of jitter

The real behavior of the data is shown in Fig. 5. Since the M-sequence has many locations with identical slopes and we only respect a finite number of experiments in our calculation, we get a cloud of data samples. By fitting (11) to this cloud, we finally arrive at the wanted rms jitter value φ_T of the device. Fig. 5 (a) relates to an example where the additive noise dominates while Fig. 5 (b) also shows some jitter induced effects.

The two examples show that the timing concept according to Fig. 3 provides very low jitter values owed to the high-speed/steep edge binary divider and the large clock rates f_c.

Moreover, the binary divider also provides perfectly equidistant strobe pulses of $s(t)$ (random jitter not respected) since it is running through all its states before it releases a new sampling event. Hence, any asymmetry of the internal flip-flops impacts all sampling pulses in the same fashion. Thus, a precise device

internal time axis is guaranteed also for a very long signal if the clock-generator is sufficiently time stable.

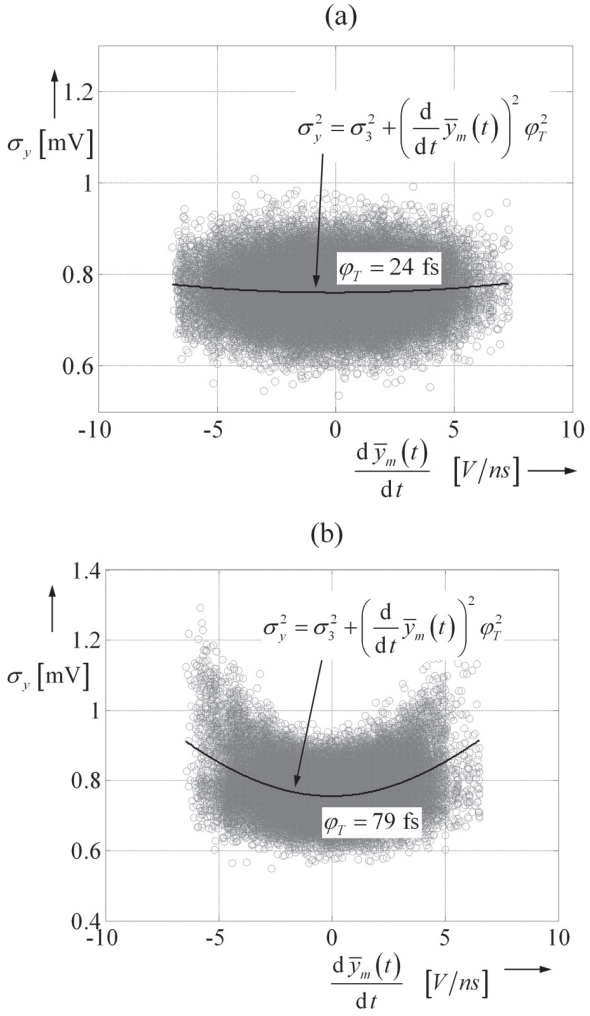

Fig. 5. Variance of measured data samples as a function of signal slope for two different RF-clock generators: (a) – High-quality RF-laboratory generator SMP04 (R&S); (b) – free running DRO

4. SUPPRESSION OF NOISE AND JITTER

Since the involved UWB signals are expanded in time (Fig. 3 (a)), the estimation of the delay time $\Delta\tau$ of a DUT requires the determination of the peak position of the correlation function between input- and output signal. In the best case, the statistical confidence in this peak position may be estimated from eq. (4). This still requires the evaluation of the SNR-value of the correlation function $C_{y_m,x}(\tau)$ which we consider as a random process while the stimulus signal $x(t)$ is supposed to be perfectly known:

$$\underset{\sim}{C}_{y_m x}(\tau) = \frac{1}{T}\int_T \underset{\sim}{y}_m(t)\, x(t+\tau)\, dt \tag{12}$$

The SNR-value of the correlation function can be defined by the relation between its peak value and its variance according to:

$$SNR_C(\tau) = \frac{\left\| \mathrm{E}\left\{\underset{\sim}{C}_{y_m x}(\tau)\right\}\right\|_\infty^2}{\mathrm{var}\left\{\underset{\sim}{C}_{y_m x}(\tau)\right\}} \tag{13}$$

whereat $\|\cdots\|_p$ means the Lp-norm.

Inserting eq. (8) into eq. (12), we get for the expected value of the correlation function:

$$\begin{aligned}\mathrm{E}\left\{\underset{\sim}{C}_{y_m x}(\tau)\right\} &= \frac{1}{T}\int_T x(t-\Delta\tau)\, x(t+\tau)\, dt \\ &= C_{xx}(\tau-\Delta\tau)\end{aligned} \tag{14}$$

and its maximum value equals the power of the sounding signal:

$$\left\| \mathrm{E}\left\{\underset{\sim}{C}_{y_m x}(\tau)\right\}\right\|_\infty = C_{xx}(0) = \|x(t)\|_2^2 = x_{rms}^2 \tag{15}$$

In Lp-norm notation, the variance of the correlation function may be expressed as follows (see [8] for details):

$$\begin{aligned}&\mathrm{var}\left\{\underset{\sim}{C}_{y_m x}(\tau)\right\} \\ &= \frac{1}{T\ddot{B}_n}\left(\sigma_3^2 \|x(t)\|_2^2 + \varphi_T^2 \|x(t+\tau)\,\dot{x}(t)\|_2^2\right) \\ &\quad using\ \frac{\mathrm{d}x(t)}{\mathrm{d}t} = \dot{x}(t)\end{aligned} \tag{16}$$

$\ddot{B}_n$ is the double sided noise bandwidth of the receiver and T is the time over which the integration is performed. Insertion of eqs. (15) and (16) into eq. (13) results in:

$$SNR_C(\tau) = \frac{T\ddot{B}_n \|x(t)\|_2^4}{\sigma_3^2 \|x(t)\|_2^2 + \varphi_T^2 \|x(t+\tau)\,\dot{x}(t)\|_2^2} \tag{17}$$

After some manipulations, we can rewrite eq. (17) in the form:

$$SNR_C(\tau) = \frac{T\ddot{B}_n}{\frac{CF^2}{SNR_0} + \frac{SAF^2(\tau)}{RJR}} \tag{18}$$

This equation is valid for compact as well as time extended UWB-signals. The involved parameters describe characteristic properties of the test signal as well as of the measurement procedure. The crest or peak factor is defined as:

$$CF = \frac{\|x(t)\|_\infty}{\|x(t)\|_2} \tag{19}$$

It may tend towards 1 for time extended signals. An ideal M-sequence has $CF = 1$. An $f_c/2$ band limited M-sequence has $CF \approx 2...3$ depending on the filter. For short pulse signals it tends to large values (the same is true for Gaussian noise). The slope amplitude factor $SAF(\tau)$ describes the coincidences of strong signal variations at large magnitude. It is defined as:

$$SAF(\tau) = t_r \frac{\|x(t+\tau)\,\dot{x}(t)\|_2}{\|x(t)\|_2^2} \tag{20}$$

Usually it depends on the time lag τ. In the case of short pulse signals, it takes high values where signal edges appear and it becomes zero at the pulse base [8, 14]. In contrast, it is nearly constant at $SAF \approx 3$ for a band limited M-sequence. The SNR-value of the captured signal with additive noise, we write as:

$$SNR_0 = \frac{\|y(t)\|_\infty^2}{\sigma_3^2} \quad (21)$$

Note that we take the peak power of the signal but not the average power for this definition. And finally, we still have the rise-time jitter ratio (t_r – rise time), which reads as:

$$RJR = \frac{t_r^2}{\varphi_T^2} \quad (22)$$

It represents a kind of "signal to noise ratio" of the time axis.

We can observe from eq. (18) that for short, pulse like sounding signals the correlation gain TB_n will be compensated by large CF - and SAF -values. The correlation will not bring any profit for noise and jitter suppression. In the case of PN-sequences, CF and SAF take small and constant values. That means, the correlation performs a suppression of additive noise and jitter as well. The jitter energy is equally distributed over the whole correlation function such that its steep edges are not more severely affected by random perturbations than flat regions. In consequence, we get a strong reduction of positions errors according to eqs. (3) or (4). The examples listed in sections 5 and 6 of this paper indicate values of 3...5 fs time position variation, i.e. a 1...1.6 μm range uncertainty in air.

This temporal stability of the measurements is the prerequisite to subtract in a stable and precise way the surface reflex according to Fig. 2 in order to make visible the weak hidden scatterer. Supposing the surface reflex must be reduced by the factor N when subtracting a reference signal, the temporal uncertainty φ_T of time position has to meet the condition:

$$\frac{\varphi_T}{t_r} \approx \varphi_T \; \ddot{B} \le \frac{1}{N} \quad (23)$$

Herein, $\ddot{B}$ is the two sided bandwidth of the surface reflex and t_r is its rise time.

5. SUPPRESSION OF DRIFT

Time drift is a long-term fluctuation which is not respected by the consideration in sections 3 and 4. It may be provoked by biased threshold voltages or trigger signals whereat the bias typically depends on temperature, aging, etc. In order to suppress drift effects, it is recommended to perform relative measurements between two receivers of identical construction and identical temperature level. These conditions are best met by integrated circuits.

Further, we should also take the temperature sensitivity of feeding cables into account. If we simply consider the coefficient of thermal expansion of copper ($\alpha \approx 16 \cdot 10^{-6}\ K^{-1}$) as an equivalent for the cable expansion and omit the temperature dependency of the dielectric insulator etc., we already get a time drift of $\Delta t \approx 100\ fs/m\,K$ for a cable of 1 m length and 1 Kelvin temperature variation. We can learn from this estimation that simply the geometric dimension of a measurement device or arrangement may limit the achievable measurement precision.

Fig. 6 shows a practical example. During the warming up phase of a device the length of its cable was measured whereat only the temporal fluctuations of the input and output signal was registered. If we only refer to the pulse position captured by the two measurement channels, we can observe a variation of about 2 ps during the observation time. This corresponds to a range uncertainty of several hundred μm in air. As expected, the variations in both channels are nearly coherent. Hence, if we account only for their differences, we get a considerable improvement of the delay time measurement to about 5 fs rms value of short time variations.

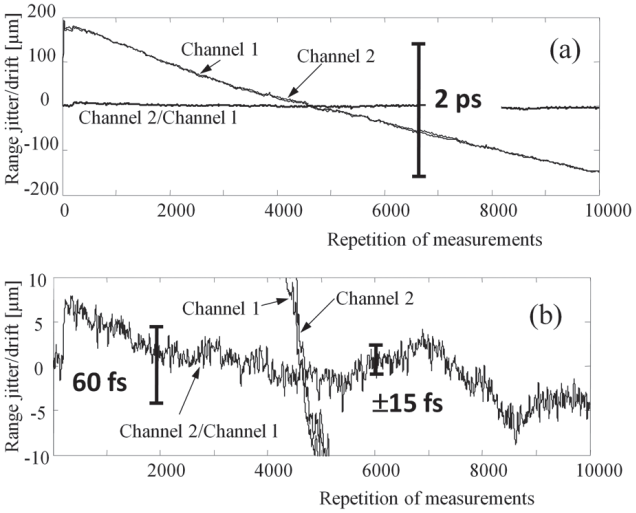

Fig. 6. Pulse position drift of an M-sequence device (9th order M-sequence, clock rate 9 GHz) during warming up observed over about 10 min. (a) – overview (b) zoom

6. DENSITY OF DATA SAMPLING

There is often the argument to sample the data very densely in order to get high range precision. This statement is not valid if it is expressed in that generic way. As we have seen in eqs. (3) and (4), bandwidth and noise are the key issues. Basically, Nyquist sampling is sufficient to reach full precision since interpolation to an arbitrary fine degree can be done in the numerical domain. However, this supposes that aliasing components must be fully suppressed. If one cannot sufficiently suppress aliasing components, the sampling rate has to be increased at least to such a degree where the aliasing components fall below the noise level. Fig. 7 demonstrates how aliasing affects the delay time measurement. For demonstration, a mechanical delay line increases the propagation path length in 2 mm steps. The measurement device was based on a 9th order M-sequence and 18 GHz clock rate using insufficient suppression of aliasing frequencies. The standard deviation of the individual distance measurements was about 1.0 ... 1.2 μm, i.e. it is more than two orders better than the systematic deviations caused by aliasing as shown in Fig. 7. The annex gives a simplified consideration about the creation of time position errors due to aliasing.

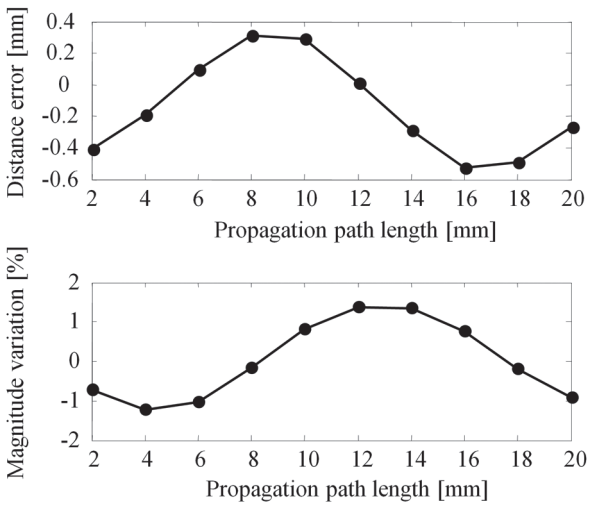

Fig. 7. Effect of aliasing onto systematic range deviations and onto the maximum value of the correlation function in dependence from the propagation path length

7. SUMMARY

Time and range accuracy should be considered with some care under UWB conditions since geometric dimensions of the object and temporal duration of signals make unique definitions of points and distances difficult. This may cause systematic deviations exceeding even the range resolution predicted by the classical formula $\delta_R = c/2B$.

The short time instabilities of an M-sequence device allow to resolve motions of a single target down to 1 μm being about 10.000 times better than the range resolution δ_R. In order to exploit this sensitivity in practical applications, the issues of mechanical precision and stability of sensor elements as well as questions of thermal expansion will become more and more important for sensor design. Aliasing effects should be properly suppressed in order to reduce systematic deviations of the device down to the level of random errors. The quality of the RF-clock generator decides about the precision of the device internal time axis with respect to absolute and random deviations. Its phase noise becomes as more influence as longer the DUT delay is.

References

[1] *M. Helbig, M. A. Hein, U. Schwarz et al.*, "Preliminary investigations of chest surface identification algorithms for breast cancer detection," in International Conference on Ultra-Wideband, Hannover (Germany), 2008.

[2] *J. Sachs, M. Helbig, R. Herrmann et al.*, "Remote Vital Sign Detection for Rescue, Security, and Medical Care by Ultra-Wideband Pseudo-Noise Radar," *Ad Hoc Networks*, 2012.

[3] *J. Rovňáková, and D. Kocur*, "TOA Estimation and Data Association for Through-Wall Tracking of Moving Targets," *EURASIP Journal on Wireless Communications and Networking,* vol. 2010, 2010.

[4] *R. Herrmann, J. Sachs, K. Schilling et al.*, "12-GHz Bandwidth M-Sequence Radar for Crack Detection and High Resolution Imaging," in International Conference on Ground Penetrating Radar (GPR), Birmingham, UK, 2008.

[5] *R. Herrmann, J. Sachs, and P. Peyerl,* "System evaluation of an M-sequence ultra wideband radar for crack detection in salt rock," in International Conference on Ground Penetrating Radars (GPR), Ohio (Columbus), 2006.

[6] *R. Herrmann*, "M-sequence based ultra-wideband radar and its application to crack detection in salt mines," Faculty of Electrical Engineering and Information Technology, Ilmenau University of Technology (Germany), Ilmenau, 2011.

[7] *J. Sachs, P. Peyerl, P. Rauschenbach et al.*, "Characterizing Impulse radiating Antennas by an Intuitive Approach," *Ultra-Wideband, Short-Pulse Electromagnetics 7*, F. Sabath, E. L. Mokole, U. Schenk *et al.*, eds., pp. 334-41: Springer, 2007.

[8] *J. Sachs,* Handbook of Ultra-Wideband Short-Range Sensing - Theory, Sensors, Applications, Berlin: Wiley-VCH, November 2012.

[9] *D. Lamensdorf, and L. Susman,* "Baseband-pulse-antenna techniques," Antennas and Propagation Magazine, IEEE, vol. 36, no. 1, pp. 20-30, 1994.

[10] *M. R. Hoseini, X. Wang, and M. J. Zuo,* "Estimating ultrasonic time of flight using envelope and quasi maximum likelihood method for damage detection and assessment," Measurement, vol. 45, pp. 2072–2080, 2012.

[11] *S. Guowei, R. Zetik, Y. Honghui et al.,* "Time of arrival estimation for range-based localization in UWB sensor networks," in Ultra-Wideband (ICUWB), 2010 IEEE International Conference on, 2010, pp. 1-4.

[12] *J. Sachs, H. C. Fritsch, M. Helbig et al.,* "Ultra-Wideband Pseudo-Noise Sensors," in Noise Radar Technology, Yalta, Crimea (Ukraine), 2012.

[13] *B. Streng,* "Entwicklung und Implementierung eines Messplatzes zur Charakterisierung des HF-Teils von M-Sequenzmesskцpfen in MATALB," Faculty of Electrical Engineering and Information Technology, Ilmenau University of Technology, Ilmenau, 2009.

[14] *J. Sachs, M. Helbig, R. Herrmann et al.*, "On the Range Precision of UWB Radar Sensors," in IRS 2010 International Radar Symposium, Vilnius (Lithuania), 2010.

ANNEX: POSITION ERROR CAUSED FROM ALIASING COMPONENTS

We assume the test signal

$$x_0(t) = \mathrm{sinc}(B_0 t), \tag{24}$$

having a rectangular spectrum of width B_0. Our measurement system is designed for this bandwidth, i.e. the sampling rate is selected to $f_s = B_0$. Sub-sampling is omitted here for the sake of brevity.

In order to emulate aliasing, we insert a second signal exceeding the given band limitation:

$$x(t) = (1-\eta)\mathrm{sinc}(tB_0) + \eta\,\mathrm{sinc}(2tB_0) \tag{25}$$

Its spectrum is depicted in Fig. 8. Part A represents the wanted signal and the parts B refer to the aliasing components after the signals is sampled with frequency f_s. The orginal spectrum of $x(t)$ spectrum is:

$$X(f) = \frac{1}{B_0}\left((1-\eta)\,\mathrm{rect}\left(\frac{f}{B_0}\right) + \frac{\eta}{2}\,\mathrm{rect}\left(\frac{f}{2B_0}\right)\right). \tag{26}$$

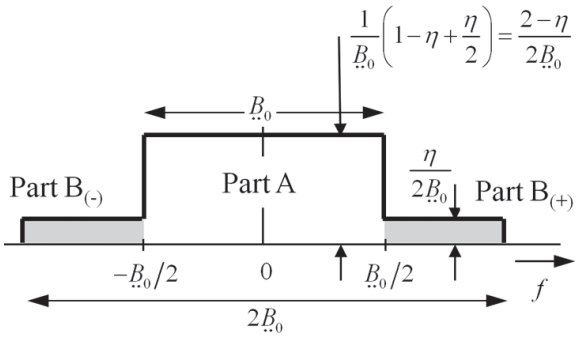

Fig. 8. Spectrum of the idealized signal

The maximum of $x(t)$ is $\|x(t)\|_\infty = 1$ and it is located at $t = 0$. Further this signal is subjected to a time delay τ, so that its maximum is now placed at time position $t = \tau$. Time signal and spectrum are:

$$\begin{aligned} y(t) &= x(t-\tau) \\ &= (1-\eta)\,\mathrm{sinc}\left((t-\tau)\underline{B}_0\right) + \eta\,\mathrm{sinc}\left(2\underline{B}_0(t-\tau)\right) \end{aligned} \tag{27}$$

$$\begin{aligned} \underline{Y}(f) &= X(f)\,e^{-j2\pi f\tau} \\ &= \frac{e^{-j2\pi f\tau}}{\underline{B}_0}\left((1-\eta)\,\mathrm{rect}\left(\frac{f}{\underline{B}_0}\right) + \frac{\eta}{2}\,\mathrm{rect}\left(\frac{f}{2\underline{B}_0}\right)\right) \end{aligned}$$

The sampled signal is then written as:

$$\begin{aligned} z(t) &= \sum_n y(n\,\Delta t_s) \\ \underline{Z}(f) &= f_s \sum_m \underline{Y}(f - m f_s) \end{aligned} \tag{28}$$

Hence, we get for our simple example:

$$\begin{aligned} \underline{Z}(f) &= \frac{f_s}{\underline{B}_0}\sum_m e^{-j2\pi(f-mf_s)\tau}\cdots \\ &\cdots\left((1-\eta)\,\mathrm{rect}\left(\frac{(f-mf_s)}{\underline{B}_0}\right) + \frac{\eta}{2}\,\mathrm{rect}\left(\frac{(f-mf_s)}{2\underline{B}_0}\right)\right). \end{aligned} \tag{29}$$

If the sampling rate is $f_s = \underline{B}_0$, the spectral components beyond $|f| \geq \underline{B}/2$ (parts B) will overlap with the central part (part A) of the spectrum. The spectrum of the sampled signal is illustrated for $m = -1, 0, 1$ in Fig. 9 for the case $f_s = \underline{B}_0$:

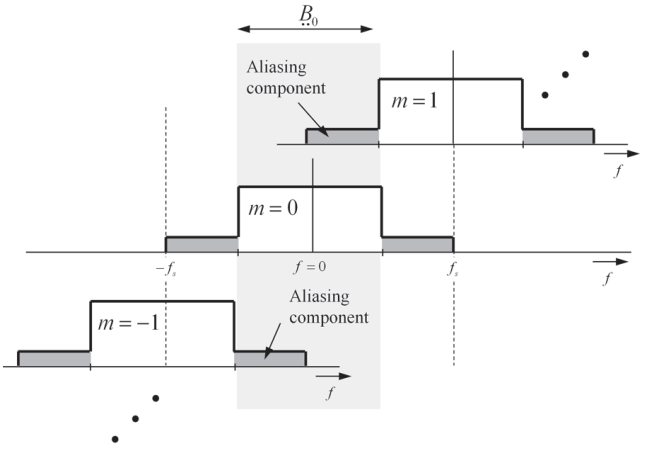

Fig. 9. Amplitude spectrum of the sampled signal fragmented in its individual part

Note, that in case of a discrete Fourier transform, only the spectral components covered by area $\pm\underline{B}_0/2$ around $f = 0$ are involved. Here, the parts $B_{(+)}$ and $B_{(-)}$ (gray) (compare Fig. 8) of the spectrum represent aliasing components caused from the spectral power exceeding the band limits $\pm f_s/2$. They are convolved into the main spectral part. The overall spectrum within this area may be written as:

$$\begin{aligned} \underline{\hat{Z}}(f) = &\underbrace{\frac{2-\eta}{2\underline{B}_0}e^{-j2\pi f\tau}}_{\text{part A effect - wanted}} + \underbrace{\frac{\eta}{2\underline{B}_0}e^{-j2\pi\tau(f-f_s\,\mathrm{sgn}(f))}}_{\text{part B effect - aliasing}} \\ &f \in \left[-\frac{f_s}{2};\frac{f_s}{2}\right] \end{aligned} \tag{30}$$

In time domain, eq. (30) gives after inverse Fourier transform:

$$\begin{aligned} \hat{z}(t) &= \int_{-f_s/2}^{f_s/2} \underline{\hat{Z}}(f)\,e^{j2\pi ft}\,df = \hat{z}_A(t) + \hat{z}_B(t) \\ &= \left(1-\frac{\eta}{2}\right)\mathrm{sinc}\left(\underline{B}_0(t-\tau)\right)\cdots \\ &\cdots + \frac{\eta}{2}\cos\frac{\pi\underline{B}_0(t+3\tau)}{2}\,\mathrm{sinc}\frac{\underline{B}_0(t-\tau)}{2} \end{aligned} \tag{31}$$

The maximum position of this signal is determined from the zero-crossing of its derivative:

$$\left.\frac{\mathrm{d}\,\hat{z}(t)}{\mathrm{d}\,t}\right|_{t=\tau} = 0 \tag{32}$$

In order to simplify the calculation, we develop $\hat{z}(t)$ into a Taylor series around the expected maximum $t \approx \tau$:

$$\begin{aligned} \hat{z}(\tau+\Delta t) &\approx a_0 + a_1\Delta t + a_2\Delta t^2 \\ a_0 &= 1 + \frac{\eta}{2}\left(\cos(2\pi\underline{B}_0\tau) - 1\right) \\ a_1 &= -\frac{\eta\pi\underline{B}_0\sin(2\pi\underline{B}_0\tau)}{4} \\ a_2 &= -\frac{(\pi\underline{B}_0)^2}{12}\left(\eta\left(\cos(2\pi\underline{B}_0\tau) - 1\right) + 2\right) \end{aligned} \tag{33}$$

whereat Δt represents the difference to τ. This gives for the maximum location:

$$\begin{aligned} \frac{\mathrm{d}\,\hat{z}(\tau+\Delta t)}{\mathrm{d}\,\Delta t} &= a_1 + 2a_2\Delta t = 0 \\ \Rightarrow \Delta t_{\max} &= -\frac{a_1}{2a_2} \\ &= -\frac{3\eta\sin(2\pi\underline{B}_0\tau)}{2\pi\underline{B}_0\left(\eta\left(\cos(2\pi\underline{B}_0\tau) - 1\right) + 2\right)} \\ &\approx -\frac{3\eta}{4\pi\underline{B}_0}\sin(2\pi\underline{B}_0\tau) \quad \textit{since} \quad \eta \ll 1 \end{aligned} \tag{34}$$

$\Delta t_{\max}$ represents the measurement error of roundtrip time provoked by the aliasing effects. As we can observe, the aliasing effect will cause a systematic error which oscillates around the actual value in dependence of the propagation time τ. The magnitude of the oscillation depends on the bandwidth and the suppression of the aliasing components.

The amplitude of the maximum is also affected by an oscillation of the same kind. Usually, the condition $\eta \ll 1$ is met, so that we can write:

$$\tilde{z}\left(\Delta t_{\max}\right)\Big| \approx 1 + \frac{\eta}{2}\left(\cos\left(2\pi \ddot{B}_0 \tau\right) - 1\right) \qquad (35)$$

Manuscript received November, 29, 2012

Juergen Sachs, for photograph and biography, see this issue, p. 87.

Ralf Herrmann, for photograph and biography, see this issue, p. 87.

Martin Kmec, for photograph and biography, see this issue, p. 88.

УДК 621.37

Точность по времени и дальности сверхширокополосного псевдошумового радара для малых дальностей / Ю. Сакс, Р. Херманн, М. Кмец // Прикладная радиоэлектроника: науч.-техн. журнал. – 2013. – Том 12. – № 1. – С. 105–113.

Оценка времени и дальности, основанная на измерениях с использованием сверхширокополосных (СШП) сигналов, должна быть внимательно рассмотрена с учетом точности, поскольку дальность, время распространения и позиция во времени часто не могут быть однозначно оценены. Данная работа иллюстрирует эти особенности и показывает некоторые общие подходы к оценке времени и дальности в СШП измерениях. Представлены ошибки измерения дальности, вызываемые сенсором, и показаны возможности, предоставляемые концепцией псевдо-шумового радара. Они обеспечивают отличную точность по оси времени благодаря использованию стабильного генератора тактовой частоты. Случайные ошибки оценки времени составляют величины порядка фемтосекунд благодаря использованию принципа устойчивой синхронизации и уменьшению дрожания с помощью корреляции. Кроме того, рассмотрено влияние дискретности спектра на точность измерения времени.

Ключевые слова: псевдослучайный сигнал, джиттер, временная позиция, точность по дальности, корреляция, влияние дискретности.

Ил. 9. Библиогр.: 14 назв.

УДК 621.37

Точність за часом та дальністю надширокосмугового псевдошумового радару для малих дальностей / Ю. Сакс, Р. Херманн, М. Кмец // Прикладна радіоелектроніка: наук.-техн. журнал. – 2013. – Том 12. № 1. – С. 105–113.

Оцінка часу і дальності, заснована на вимірах з використанням надширокосмугових (НШС) сигналів, повинна бути уважно розглянута з урахуванням точності, оскільки дальність, час поширення та позиція в часі часто не можуть бути однозначно оцінені. Дана робота ілюструє ці особливості і показує деякі загальні підходи до оцінки часу і дальності в НШС вимірах. Представлено помилки виміру дальності, що викликаються сенсором, і показано можливості, що надаються концепцією псевдошумового радара. Вони забезпечують відмінну точність по осі часу завдяки використанню стабільного генератора тактової частоти. Випадкові помилки оцінки часу складають величини порядку фемтосекунд завдяки принципу стійкої синхронізації та зменшення тремтіння за допомогою кореляції. Крім того, розглянуто вплив дискретності спектра на точність вимірювання часу.

Ключові слова: псевдовипадковий сигнал, джіттер, часова позиція, точність за дальністю, кореляція, вплив дискретності.

Іл. 9. Бібліогр.: 14 найм.